Methods of minimizing additional amplitude and phase noise on diode lasers caused by acousto-optical modulators

Bachelorarbeit in Physik
von
Johannes Schmidt

angefertigt im Physikalischen Institut,
vorgelegt der Mathematisch-Naturwissenschaftlichen-Fakultät
der
Rheinischen Friedrich-Wilhelms-Universität
Bonn

September 2019

Ich versichere, dass ich diese Arbeit selbstständig verfasst habe und keine anderen als die angegebenen Quellen und Hilfsmittel benutzt sowie die Zitate kenntlich gemacht habe.

I hereby declare that this thesis is my own work and that no sources or tools other than those cited were used.

Bonn,..... .....

Date Signature

1. Gutachter: Prof. Dr. Michael Köhl
2. Gutachter: Priv.-Doz. Dr. Elisabeth Soergel

Contents

1 Introduction

Bad acoustic speakers, electrical instruments, optical instruments, etc. No matter for which purpose, when working with any kind of signal, it always has to be large enough, relative to the always present noise. This is also true for lasers, especially with low power. In the research group of Professor Köhl, ultra-cold atomic Fermi gases are employed to study the many-body physics of quantum gas. After cooling they use optical traps to keep ^{40}K atoms in place.
Lasers, forming standing waves, act like a periodic potential and therefore behave like a very fine adjustable solid. However, fluctuations in the phase and intensity of the lasers cause vibrations of the atoms and therefore heat them up again. This can be problematic since the atoms need to be prepared close to the ground state. So there is a limit of cooling given by the noise on the used laser.

For a precise adjustment of the laser frequency and more importantly the intensity one can use acusto-optical modulators (AOM) . These devices, however, can cause a significant increase of the noise, depending on the radio frequency (RF) signal driving them. Therefore, the source of the high frequency signal which drives the AOM will be exchanged in this thesis. For this two printed circuit boards using a technology called direct digital synthesis were used and integrated into a compact setup. They provide independent frequency, phase, and amplitude control on every one of its channels. In order to communicate with it they were connected to a Raspberry Pi and controlled by a program written in python that uses an interface bus called serial peripheral interface.

At the end of this thesis the results were measured with a laser diode, by comparing the intensity and phase noise of the old, current and new setup used in the ^{40}K Fermi experiment. For this the RF signal chain is adjusted to produce comparable results, for all different setups tested in this thesis.

2 Theoretical Background

First some theoretical background to lay the foundation for the thesis.

2.1 What is noise?

Noise is often understood as an additional random fluctuation on a signal. It can be acoustic, chemical, electrical, optical, etc. If someone is talking about noise though, it's not just random, but also unwanted. So for example, if some electrical measuring device trying to measure a constant DC signal and picks up the 50 Hz and its harmonics of the main voltage supply it is also called noise. In this example the 50 Hz are not random, since the source of this signal is known, nevertheless it is unwanted. So noise is everything that obstructs, hides or diminishes a wanted signal. In this thesis electrical noise will play an important role.

2.1.1 Electrical noise

Electrical noise, in principle, is caused by only two phenomena. When investigating the definition of current flow the following definition can be found.

$$\vec{J} = \rho\,\vec{v} = n\,e\,\vec{v} \tag{2.1}$$

Here $\vec{v}$ is the direction and amount of the velocity and ρ is the charge density. It can also be written as the product of a charge carrier density n and the charge of the electron e. Taking the derivative with respect to time one obtains:

$$\frac{\mathrm{d}}{\mathrm{d}t}\vec{J} = e\,\vec{v}\,\frac{\mathrm{d}}{\mathrm{d}t}n + n\,e\,\frac{\mathrm{d}}{\mathrm{d}t}\vec{v} \tag{2.2}$$

So the only sources for noise are either fluctuation in density or fluctuation in velocity of the current flow.

One might ask where the randomness comes from, if noise is only caused by this two reasons. The answer is, there are many ways of varying these two properties.
One very physical example for the fluctuation of the velocity of the current flow is thermal noise, also called **Johnson-Nyquist noise**. Johnson did the experiment and Nyquist calculated the analytical expression for the phenomena [3]. It is caused by the thermal agitation of the charge carriers, which are usually electrons. The bigger the current flow is, the more voltage drops on resistors. So they become hotter and this drives the Brownian motion of the charge carrier in it and since moving charges are defined as current an additional signal is added.
The next example is caused by irregularities in the charge density. It is called **shot noise** and its caused by the quantised nature of the charge carriers. [21]. Shot noise is observed at low currents. When one has a current flow in the region of few mA the fluctuations caused

by the quantised nature of the electron is not noticeable. However, if the current only contains a few electrons per second the fluctuation is noticeable This is a so called **quantum limit** and it is not possible to eliminate it.
This is not only the case for electrons but for photons in light as well. In the experimental setup of this thesis not only electrical noise but also optical noise, coming from a diode laser, is measured.

2.2 Noise on Diode Lasers

For the interaction of matter and light one has to chose a light source. Diode lasers are very useful tools for achieving a source with much power and relativly small bandwidths. The ^{40}K experiment uses Laser diodes for optical traps and laser cooling. The noise on these lasers in frequency and intensity can limit the lowest possible temperature. This makes intuitive sense, since a vibrating container is not able to do a good job in maintaining its entries.
This phenomena can also be shown with time dependent perturbation theory in quantum mechanics, when approximating the potential as a harmonic oscillator with an oscillating minimum. So it looks as follows,

$$V(x,t) = \frac{1}{2}m\omega^2\left[x - \epsilon x_0 \cos\left(\Omega t\right)\right]^2$$

where m is the mass of the particle, ω is the angular frequency of the particle, x_0 denotes the amplitude of the fluctuation and Ω is the angular frequency of the modulation. ϵ is a small parameter. Such a perturbation corresponds to fluctuations in the phase or frequency of the laser causing the local minimum.
Similar calculations can be done for fluctuations in the amplitude, see [25].

Electromagnetic waves have the properties frequency, amplitude and polarisation. So every of these properties can have fluctuations and therefore change the character of the wave. Polarisation of a laser can be important for driving excitation in atoms in optical pumping, spectroscopy, trapping and cooling atoms. Polarisation noise is an important topic for this applications, however it is not part of this thesis. Much more common are problems with unwanted fluctuations on amplitude and frequency. Noise on these properties is often the reason for excitation and heating of atoms.

2.2.1 Intensity noise

Intensity noise characterises the fluctuations on the output power of the laser, so is related to the amplitude [23]. There are multiple ways to measure and classify intensity noise. The easiest way of measuring it, is to record the variation of the optical power $P(t)$ with a photo diode. It can be considered as

$$P(t) = \overline{P} + \delta P(t)$$

where $\overline{P}$ is the average dc value and $\delta P(t)$ refers to the fluctuations around zero. Fluctuations can occur at different frequencies with different amplitude, therefore a power spectral density (PSD) takes that into account and can be defined as the Fourier transform of the fluctuations.

The offset of a PSD spectra, however, always depends on the dc value of the spectra. In order to take that also into account the **relative intensity noise** (RIN) $S_I(f)$ [19], which is defined as the PSD divided by the dc value.

$$S_I(f) = \frac{2}{\overline{P}^2} \int_{-\infty}^{\infty} \langle \delta P(t) \delta P(t+\tau) \rangle \exp(i2\pi f\tau)\, \mathrm{d}\tau \tag{2.3}$$

One can also calculate the root-mean-squared (r.m.s.) value, for quick comparison. It is defined via

$$\frac{\delta P}{\overline{P}}\Big|_{rms} = \sqrt{\int_{f_1}^{f_2} S_I(f)\, \mathrm{d}f}$$

This property is dimensionless. Note, that all of these definitions are statistical properties, that is the reason of the mean (angled brackets) in equation 2.3). Furthermore, it is important to specify the bandwidth of the taken measurement. This means that just a scalar without the information which frequencies were considered does not have much informative value. In a PSD plot it is automatically considered, because the bandwidth can be seen on the x-axis. The speed of the used photo diode is also an important property. It might show features in regions out of its range, however these are not caused by the detector, but by the electronics. And if the resolution is not good enough it might happen, that peaks with a smaller linewidth than the bandwidth cannot be seen.

The ambient conditions are also important to consider as noise source, some examples are other light sources, acoustical noise in the room, temperature (absolute values as well as changes during the measurement) or vibration, to name a few. Acoustic influences, for example from a air conditioning system, would cause sharp peaks in the spectra somewhere between 20 Hz and 20 kHz. Moreover, depending on the laser type, regime, cavity length, upper-state lifetime, cavity damping time and some more properties result in changes in the pump power. This leads to so-called **relaxation oscillations** [20] which can cause peaks in the measured region. However, for diode lasers this occurs in the magnitude of GHz, so it will not be measured in this thesis. The same is true for mode beating.

There are multiple ways to improve intensity noise:
The most obvious one is to chose a laser that fits best for the application and operate it with the optimal parameters. For example, if one is interested in cooling atoms as much as possible, it is not a good choice to use a laser with a relaxation oscillation near to a resonance of the atom.
Further, reducing environmental influences is also helpful, such as using vibration isolation tables, quiet air-condition, no external light sources in the room where the experiment is

installed. Also stable current and temperature conditions of the laser are important (see section 2.2.3)
Another method uses electrical regulators. This was not achieved in this thesis, see section 7. The quantum limit of intensity noise is given by quantisation/shot noise.

2.2.2 Phase noise

Phase noise is related to fluctuations of the frequency and the phase. Both of these properties are closely related to each other. They both can cause an increment of the laser linewidth. For this definition of phase noise single-frequency lasers are considered. If a laser has multiple modes the definition of phase noise has to be specified differently [23].
Phase noise can also be described with a PSD. From this, one can determine the FWHM (full width half maximum) or the position of side peaks. The peak might even have a non-lorentzian shape. The measurement of phase noise is more difficult than the measurement

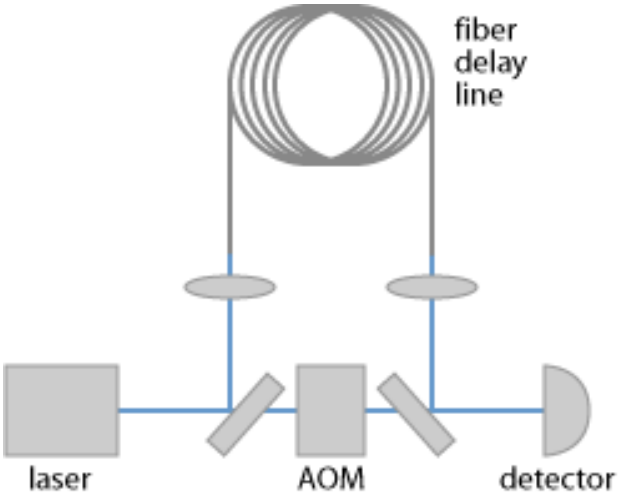

fig. 2.1: Principle experimental setup of the self-heterodyne method [23]

of intensity noise. One way to measure it is the incoherent interference of two laser beams with slightly different frequencies. This difference is often created with AOMs. These two laser beams can come from two different lasers or from one laser. If using one laser the beam has to be split into two beams, where one of them needs to propagate a larger distance as the coherence length. This can be done relatively easily with a fiber. However, this might be expensive, depending on the bandwidth of the laser, because the smaller the linewidth, the larger is the coherence length. It can go up to several kilometers. Direct observation of the linewidth of a laser can be difficult. So the interference of these signals with slightly different wavelength creates a beat note. This beat note has a frequency of exactly the difference of the laser beams, per definition. So if the difference is 200 MHz, one can easily observe it with a spectrum analyser. The linewidth of the beat note is proportional to the linewidth of the actual center wavelength. This method is called **self-heterodyne method**,

see fig. 2.1.

The quantum limit of phase noise causes random walks in the optical phase due to spontaneous emission of photons inside of the resonator. Among other things this causes the finite value of the linewidth. There is a formula that approximates the dependencies of this phenomena [26]. However, this limit of often not reached, because of other more technical limitations. One example for this are fluctuations on current and temperature of the laser diode.

2.2.3 Current and temperature controller

When buying a laser diode two important properties are specified in the data sheets, **Temperature Coefficient of Wavelength** (TCW) and **Current Coefficient of Wavelength** (CCW) . They describe how much the wavelength of the laser λ changes due to changes in current I or temperature T.

$$TCW = \frac{\mathrm{d}\lambda}{\mathrm{d}T} \quad , \quad CCW = \frac{\mathrm{d}\lambda}{\mathrm{d}I} \tag{2.4}$$

A typical value for a CCW is 3 MHz/μA [17]. So that is a huge addition of linewidth caused by relatively small fluctuations. With the TCW it is similar, so precised control of these two properties is of great interest.
When the beam of diode laser is as stable as possible the AOM, responsible for precise adjustment of the frequency and intensity, can be investigated into the experiment.

2.3 Acousto-optic modulator

Sound waves can be interpreted as dynamic periodic vibrations of the medium that it is propagating through. They consist of regions of rarefaction and compression. Since the speed of light is so much faster than the speed of sound the sound wave can be considered as static. So it behaves like a grid with distances proportional to the frequency of the sound wave. A propagating soundwave with wavelength Λ is will reflect light of wavelength λ if the angle θ between them satisfies the Bragg condition.

$$\sin\theta = \frac{\lambda}{2\Lambda} \tag{2.5}$$

Furthermore, one can find the conditions $\omega = 2\pi c\lambda^{-1}$ and $\Omega = 2\pi c\Lambda^{-1}$. When investigating the Doppler shift the following condition holds [24]

$$\omega_r = \omega \pm \Omega \tag{2.6}$$

where ω_r is the angular frequency of the reflected wave. It is plus and minus because the light wave can propagate in the direction of the sound wave or contrary to it.
In practice AOMs mostly consist of transparent solids with a glued Piezo crystal that is

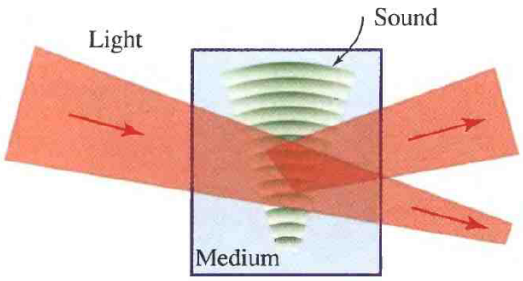

fig. 2.2: Basic principle of a AOM [24]

driven by an RF source. So the frequency of the RF signal is equal to the frequency of the sound wave Ω. This means, noise on the electrical signal gets inherited on the optical signal, due to equation 2.6.

There is however a difference between amplitude and phase modulation. Phase modulation is the intuitively expected effect on the frequency of the light, namely the shift of the center wavelength. Amplitude modulation, on the other hand, is caused by an effect on the amplitude of the light. It is observable at the frequency of the sound wave Ω. This is because the intensity of the optical wave is proportional to the intensity of the sound wave. The AOM by itself does not add noise to the optical signal, it is the RF source driving it. The signal generator build in this thesis uses a technique called direct digital synthesis.

2.4 Direct digital synthesis

Direct digital synthesis (DDS) is a method of creating, adjustable periodical signals of arbitrary shape and high precision. The basic setup can be seen in fig. 2.3. Every DDS needs a incoming clock signal. This could be a voltage controlled oscillator, a quartz crystal, a atom clock, or something else providing a RF source. The noise of the output of the DDS signal is than almost the noise of the incoming clock signal. This signal gets wired into a address counter, where every peak of the clock sent into it, iterates through a set of addresses. Each address refers to a phase of an oscillator, saved in the lookup table. This is typically the information of a sinewave in a programmable read-only-memory (PROM). These digital values are sent to a register and from there to a digital-to-analog-converter (DAC). The phase noise of this signal is basically that of the reference clock.
Since this signal is discretized one have to consider quantisation noise, aliasing, etc.[9]. In addition to that the DAC has unwanted higher harmonics. One can introduce a low-pass-filter (LPF) to deal with this. Nonetheless, this can also be a limit if one needs higher frequencies, which was not the case in this thesis.
The problem yet with this method is its inflexibility. To change the frequency of the sin one

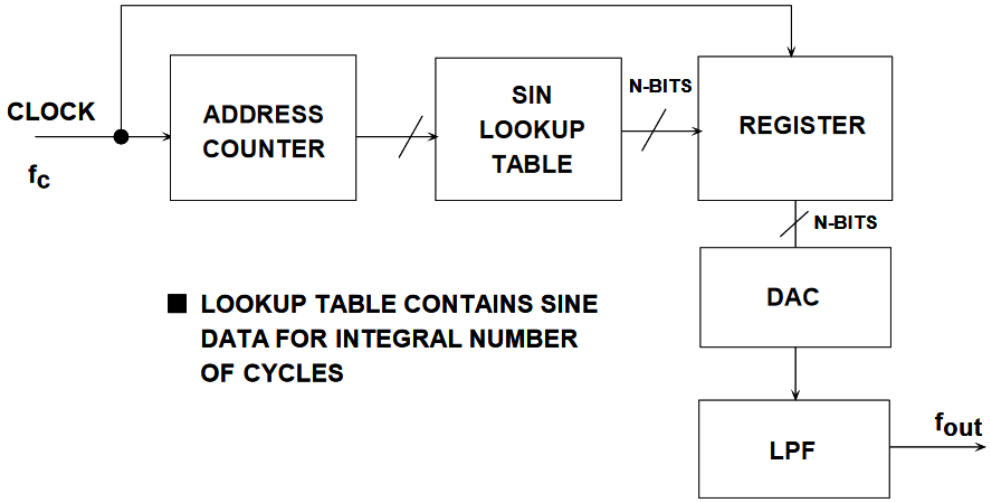

fig. 2.3: Basic structure of a DDS [9].

has to use a different address counter and lookup table. Therefore, the DDS used in practice (which I use as well) are a little bit more complicated.

Here the PROM is driven by a phase register. This depends on the so called frequency-tuning-word (FTW). The phase advance $\Delta\phi$ and output frequency f_{out} are then given by [14]

$$\Delta\phi = \frac{360^\circ}{2^n} \quad \textit{and} \quad f_{\text{out}} = \text{FTW} \cdot \frac{f_{\text{clk}}}{2^n}.$$

Here f_{clk} is the frequency of the clock and n is the number of bits of the addresse space. By adjusting the FTW one can adjust the outcomming frequency. This phase truncation adds phase noise [9].

3 DDS Box

The first part of the thesis was to build a device that uses direct digital synthesis in order to replace the RF source for the AOMs used in the Fermi experiment for the x-,y- and z-axis laser for the atom trap. The device should have eight output ports and one input port for the reference clock of the DDS.
The device should provide a way of communicating with it. This will be managed via a build in Raspberry Pi that controls the DDS and is also connected via Ethernet to the local server of the lab. More information about Raspberry Pi in the Appendix. So every computer connected to the server is able to control the Pi. The Software should be as simple as possible, so it is easy to use.

3.1 Setup

As DDS the evaluation board of the AD9959 chip from Analog Devices Inc. [18] was used. Nonetheless, this board is not enough, because it has only four outputs. So two of them were used. The AD9959 provides multiple ways to control it. One can use a USB port

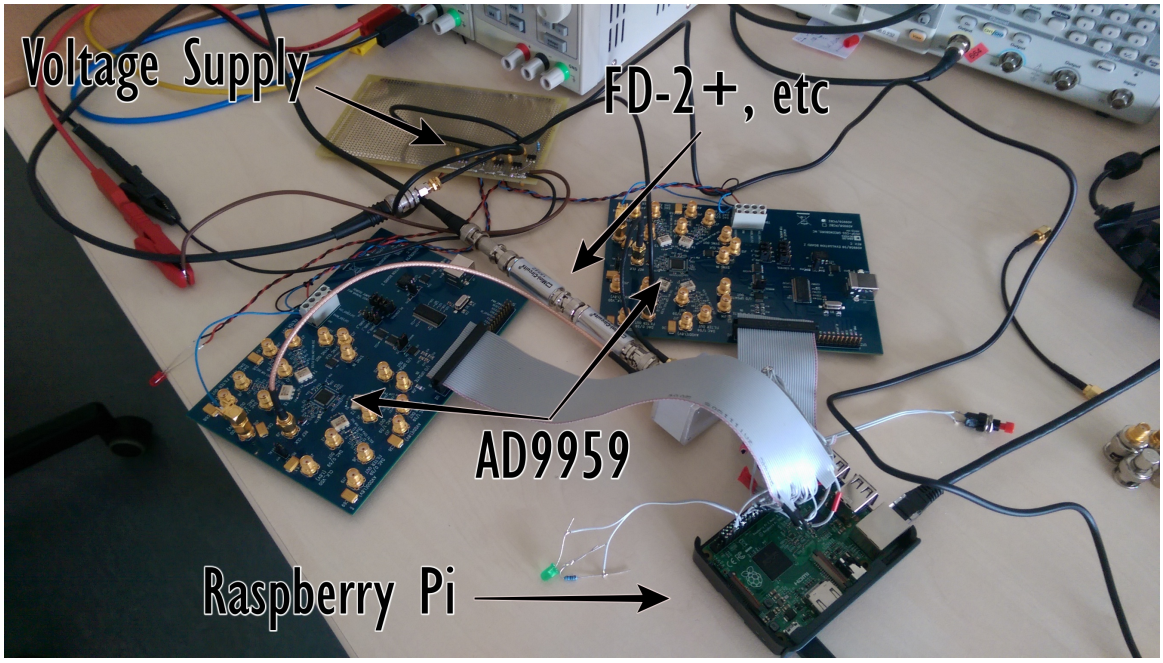

fig. 3.1: Two AD9959 evaluation boards to the Raspberry Pi. This is not the final setup.

and work with the software available on the official website. However, this is probably not comfortable enough and it becomes hard to modify slight changes in the original software. So a different approach was chosen. The AD9959 offers the possibility to communicate via SPI. The principle of SPI is explained in the Appendix.
There are different modes one can use with the AD9959. Here the 3-wire-mode, which is

explained in the data sheet, was used. Jonas Schmitz, a PhD student of the research group, already wrote the code for the control of this board with python. However, it had to be modified in order to switch between the two boards.

One has to connect seven pins for the communication of the board. They have to be connected as in table 3.1.

AD9959	Raspberry Pi
SDIO_0	MOSI
SDIO_2	MISO
SCLK	SCLK
CSB	CE 0/1
PWR_DWN	any GPIO
RESET	any GPIO
IO_UPDATE	any GPIO

Table 3.1: Pin layout for connection of AD9959 with Raspberry Pi

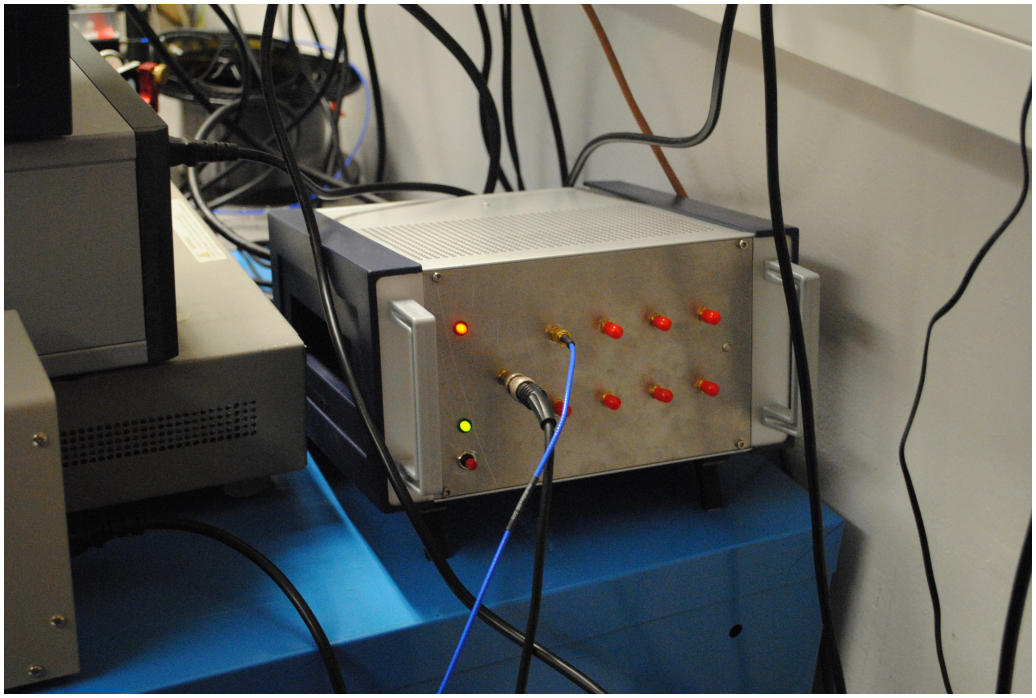

fig. 3.2: The green led acts the same as the "ACT" led on the Raspberry Pi itself, so it indicates if the Pi is on. The red led indicates that the entire board is attached to power. The button below the green led is for turning of the Pi.

Since the phase noise of the the signal emitted by the DDS is almost the phase noise of the incoming clock signal, we use a 10 MHz source of a Atom clock. It is a rubidium clock

with a accuracy and stability of a few parts of 10^{11} over periods of seconds to hours and a output power of 9.6 dBm. It is important to mention that the AD9959 has an max reference clock input level of 1000 mV and 9.6 dBm reaches almost that value.
However, the atom clock does not go directly into the AD9959. In order to reach a better resolution and therefore emit higher frequencies it a frequency multiplier, the FD-2+ from Mini Circuits [7], was used. This device doubles the incoming frequency in a wideband of 10 to 1000 MHz. The cost of it though is frequency dependent attenuation and higher harmonics. Since the goal is to feed 10 MHz, the loss caused by the FD2 is around 13 dB. However, the higher harmonics might provide problems as reference clock for the DDS. Therefore we also introduced a bandpass filter into the circuit, namely a BBP-21.4+ [6]. This causes a sufficient suppression of all the harmonics and another attenuation of about 1 dB. All this is demonstrated visually in fig. 3.3 in the measurement section.

In the end there is an additional signal splitter [8] to provide both pins with the clock, so another 3 dB has to be considered. This results in a whole loss of 17 dB and a output power of -3.4 dBms. If someone is interested in using a different RF source than the atom clock, one has to consider a max input power of 21 dBm and a min value of 7 dBm for the final setup with all listed devices. The min value is because the AD9959 has also a min input voltage of 200 mV. When we tested it, it still worked with 70 mV, but we did not do a long-term test. Maybe this can cause unstabilities, so probabely it is better to stick to the data sheets recommendation. The emitted oscillation of the DDS can than go up to -6 dBm. For someone interested into more detailed properties of the parts, see the data sheets in the references.

3.2 Problems and challenges

SPI control with spidev library on Raspberry Pi

The first idea was to connect every pin of the GPIOs to the same pins on the AD9959 evaluation board, except for the slave select pin, that controls the address of the data flow (see Appendix 8.1). Like this the information can flow to both devices and so every output can be controlled. This was indeed the case. But, when one set the frequency on the second board, the first board reset. So for some reason the communication with two boards principally worked, but not simultaneously. So I decided to decouple the wires and connect every pin on the evaluation boards to a distinct pin on the Raspberry Pi. The Pi supports multiple SPI buses at the same time. By default this is not activated though. The recommended operating system for the Pi is called Raspbian, a Debian (Unix) based operating system. In */dev* folder in Unix systems is the folder where hardware drivers are located [12]. By default one will find the files *spidev0.0* and *spidev0.1*. This means that only the 0th bus with the SS pins 0 and 1 are available. In order to activate more one has to add a command to the */boot/config.txt* file. This file gets executed when the Pi is booted, enabling the second SPI output. This might not be the most elegant way, but it worked. However, this depends on the version of the python library communicating with the Pi. At first it worked, but when

the Pi was updated , which was necessary due to lots of errors that occurred, it stopped working. So a later version of Respbian or a newer version of the spidev python package might still work with this technique. But not with the current setup. At this point jumper cables started getting used, because until that point everything was directly soldered on the devices. Not only does that take more time to change something one is also not flexible to quickly remove one pin and check what is happening, which helped a lot for debugging and figuring out the purpose of every pin. One might notice,that SPI only needs four pins, but in order to work with the AD9959 in 3-wire-mode seven pins are necessary. One of these pins, called reset, sends a signal to the board that shuts down the addressed channel before it changes it. This makes perfect sense with the fact, that it was not possible to run two boards on the first setup simultaneously. So the MISO, MOSI and SCLK of the board were wired again to the same GPIOs of the Pi, but disjoint pins were chosen for the rest. This worked fine. Even without any additional drivers or multiple SPI setups.

Current fluctuations and hard turn offs

Like on every computer the Raspberry, when it is suddenly disconnected from the power supply, can cause problems. However, there is no build in turn off button so one needs to do one by oneself. Depending on the power supply there might be noticeable voltage drops when much current flows. This can cause the same problems. The problem is, that one has no chance to debug the resulting problems. All that remains is a new attach. For this project the RS-15-5 from MEAN WELL [4] was used. The load of the two AD9959 boards and the Pi is at around 1 A, so it is actually beneath the 3 limit of the device. However, the peaks might be higher. In order to flatten the signal a capacity of 4700 μF was connected in parallel to the dc voltage supply.

3.3 Meassurements

All data in this section was measured with a *Agilent E440B ESA-E series spectrum analyser* (See the data sheet here: [27]). This device has a span resolution between 100 Hz and 26.5 GHz. It does not use a Fourier transform, but an internal signal source that is compared with the incoming signal. This results in a bandwidth that limits the resolution of the peaks depending on the chosen span, if set on auto. The two important properties of such spectrum analysers that controle this resolution are the **resolution bandwidth** (RBW) and the **video bandwidth** (VBV). Adjusting the RBW can provide lower noise floor and finer frequency resolution and adjusting the VBV will smooth the trace and makes signal identification easier. However, lowering there two properies will increase the sweep time. So its not efficient to always chose them as small as possible. That is the reason why the peaks in, for example, fig. 3.3 look so bright. The more one zooms in the smaller it gets, until the actual linewidth of the signal or the maximum bandwidth of the analyser is reached. Also note the peak a 0 Hz. This is due to a DC value coming with the signal, even though a DC block was used.

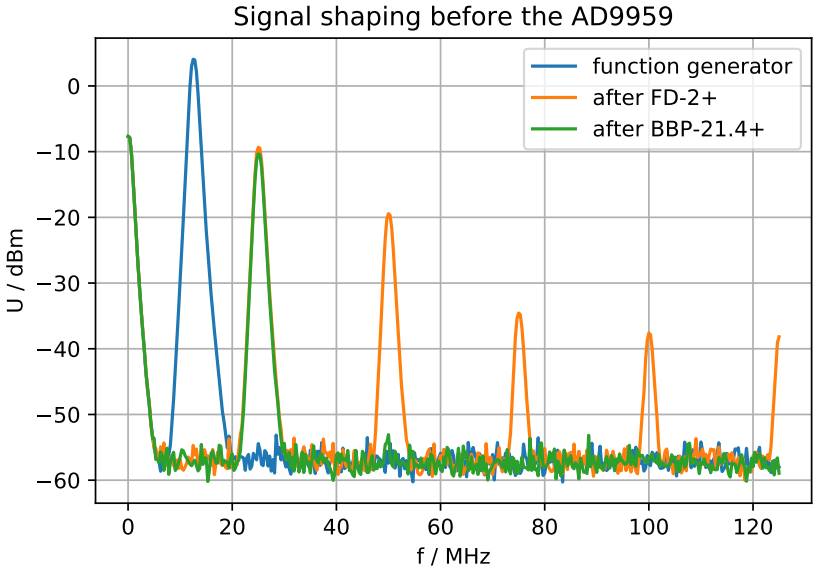

fig. 3.3: Here the spectra of the different steps of the frequency doubling are shown. The function generator was adjusted to emit 12.5 MHz. Resolution and video bandwidth = 1 MHz

The signal of the DDS is also driven through an amplifying circuit, because its output signal is not powerful enough for the AOM.

4 Amplifying circuits and different high frequency sources

4.1 AOM Driver Box for DDS Box

In order to amplify the signal, Dr. Akos Hoffmann, one research fellow of the group, build a very handy device specifically for this application. A simplified schematic of this box is shown in fig. 4.1. The idea is to have a adjustable gain with this box. It also offers

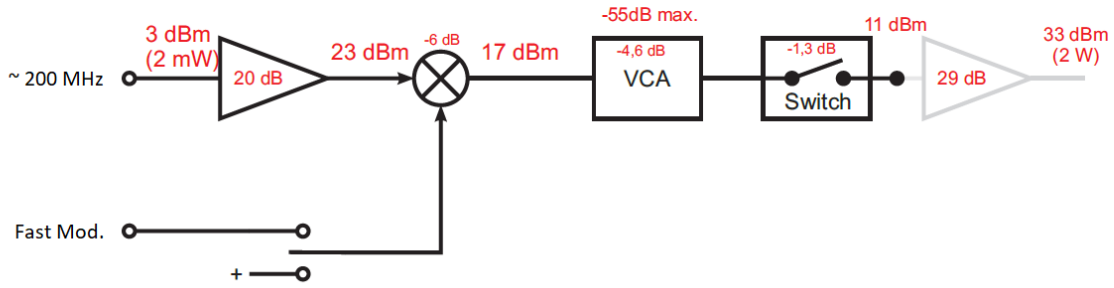

fig. 4.1: Simplified schematic of the box Dr. Akos Hoffmann build

the possibility to add modulations on the signal. This was however not used in this thesis. A potentiometer on the front panel is used for adjusting a voltage going into the voltage controlled amplifier . There are more features not covered in this thesis.

4.2 VCO Box and Marconi signal generator

The AOM driver box is a replacement for an amplified voltage-controlled oscillator (VCO) with some additional modulation functionality. A rough visualization of the VCO is shown in fig. 4.2. The main piece of it is the VCO itself. This is also the main source of noise. This signal will be amplified. After that a frequency mixer follows to offer additional modulations of the signal. Then a voltage controlled attenuator, followed by another amplifier (amp). In the old setup even this was not enough, so they used another amp which again had to be attenuated before.
The problem with this setup is that it has a lot of noise sources. Like mentioned earlier,

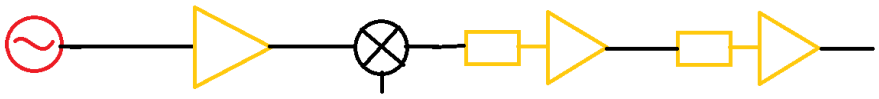

fig. 4.2: Rough schematic of the old circuit.

the worst one is the VCO (red). That is the reason why it was replaced by another function generator before this theses. The difference to the old setup has not been measured though. This is done here subsequently. The results are presented in the next subsection. Furthermore, the amps and attenuators are also a source of noise (yellow). Therefore the new circuit,introduced in the last section, was build

The *Marconi signal generator 2024* is the function generator currently used in the experimental setup of the ^{40}K experiment. For more information about this device, see the data sheets.

4.3 Measurements

When investigating the spectra of these three sources in a wider range, multiple harmonics are observable, see fig. 4.3. This is not a problem, because this frequencies are not taken by the AOM.

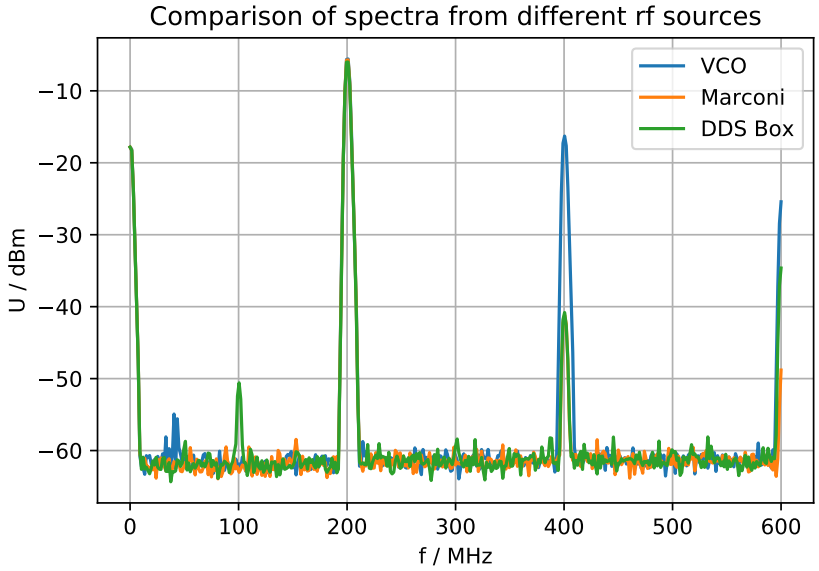

fig. 4.3: Resolution and video bandwidth = 3 MHz

When reducing the span and bandwidth on the 200 MHz peak one can already see dif-

ferences in the linewidths, see fig. 4.4. Like expected the VCO shows the widest peak,

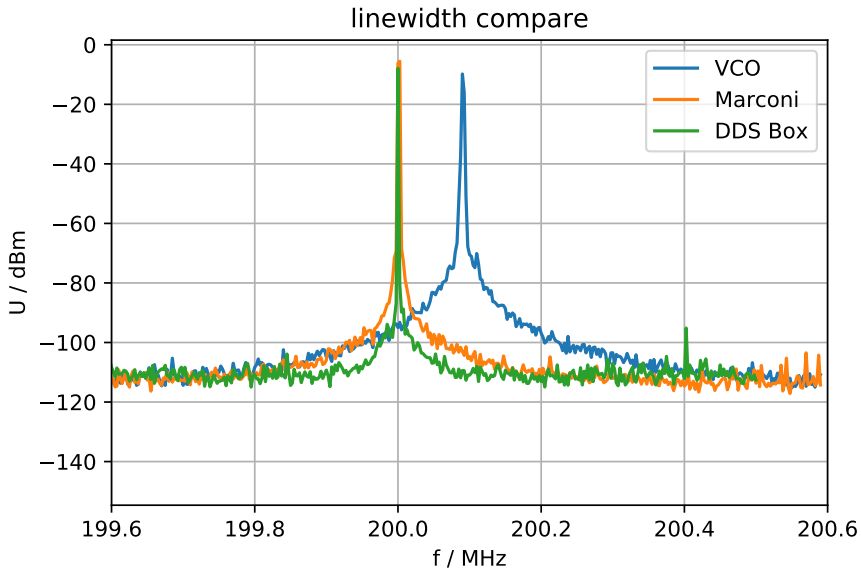

fig. 4.4: Resolution and video bandwidth = 100 Hz

however this is a dB scale. So the most fluctuations occur only at around -78 dBm, which can probably be neglected. So a closer look is necessary. Another feature can be seen in this figure. The frequency control of the VCO is managed with a potentiometer with constant sensitivity. Therefore, it is not as precised as the Marconi or DDS Box, but shows a deviation of 100 KHz in the frequency. This however might be noticeable depending on the setup. For example when one needs a very efficient coupling into a fiber of a beam that went through a AOM this might make a difference.

In order to measure the FWHM of the peaks, three separate measurements were made. See fig. 4.5. These plots are linear on both axis. Here the resolution and video bandwidth is equal to 1 Hz, so on the maximum of the spectrum analyser. Furthermore, the signal was averaged over 10 spectra.

By reading off the FWHM of the diagram one finds the following values:

Device	FWHM
VCO	~ 2 kHz
Marconi	~ 1 Hz
DDS Box	~ 1 Hz

Table 4.1: FWHM of the of the different RF sources of fig. 4.5

So there are three magnitudes of difference between the VCO and the others. Since the resolution and video bandwidth is equal to 1 Hz it is not possible to say if the linewidth of the RF sources is not even better than this, but it is definitely not worse.

Another interesting thing is the spectra of the VCO. If one compares the measured voltages, one will find that the voltage of the VCO is almost two magnitudes below the voltages of the Marconi and the DDS Box. Nonetheless, the peak in fig. 4.4 shows only a small difference. This is because the VCO showed multiple of these peaks fluctuating around 200 MHz. The Peak seen in fig. 4.5 was one of the few not moving around all the time, so it was assumed to be a main carrier.

This measuring method does not give insights into the amplitude noise. There was no possibility to measure it efficient, so I measured 40 times the peak of on the spectrum analyser to at least have an idea. The result can be seen in fig. 4.6. The only reason for the different positions of the distributions is the slightly different adjusted voltage value and attenuation caused by different screw connections. For comparing them better, the mean of each distribution was calculated and divided by each x-value, see fig.4.7.
One can guess a tendency that the DDS Box is the best and the VCO the worst, however the differences are small.

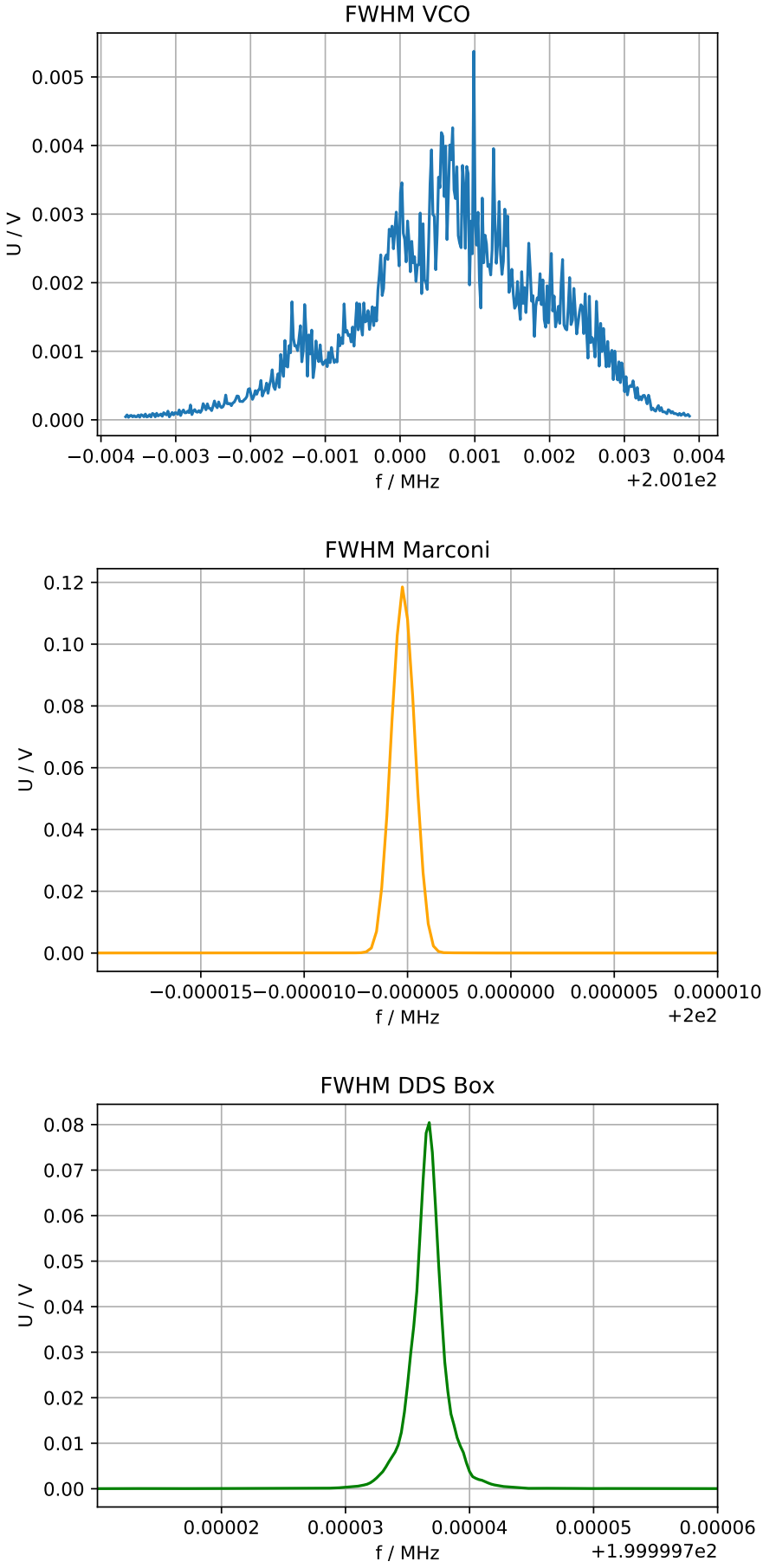

fig. 4.5: Zoom into 200 MHz of the different RF sources

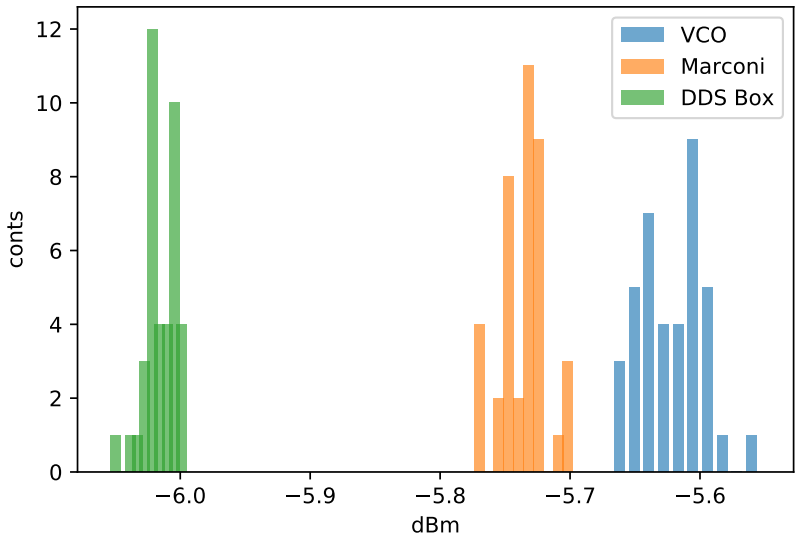

fig. 4.6: single picture mode amplitude measurement on spectrum analyser 40 data points each.

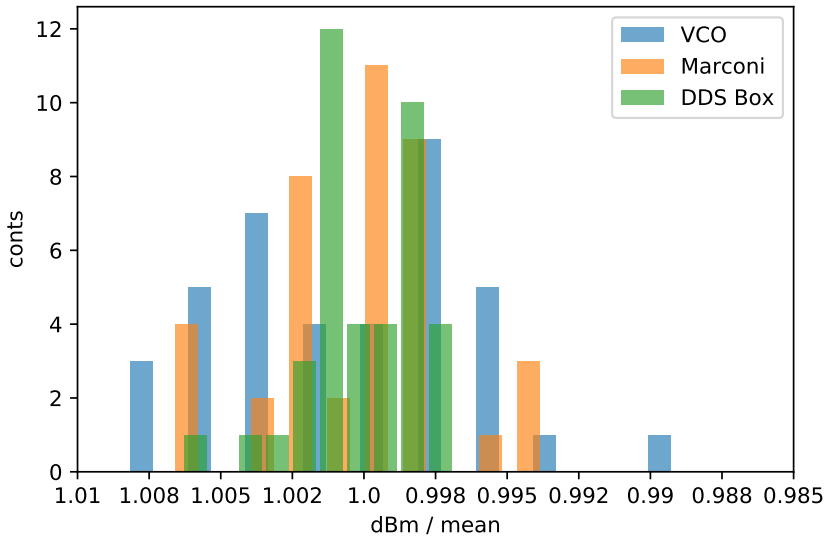

fig. 4.7: Same data as in 4.6, but divided by the mean value respectively

5 Measuring intensity noise

In the paper *Using diode lasers for atomic physics* from Carl E. Wieman and Leo Hollberg [2] there is one subsection about amplitude spectrum (II. B.). They used a photo diode and RF spectrum analyser capable of measure up to 3 GHz. They also stated that the general structure of the amplitude noise shows the most structure at the lowest Fourier frequencies at about less than 500 kHz. By observing the signal with a *Agilent E440B ESA-E* up to 1 MHz one can see that the most fluctuations are under 100 kHz, especially near zero. That is where measurements were taken.

5.1 Measuring method

Before comparing intensity noise of the different settings one need a method for measuring it. In the research group the way for doing so is to use an old *HP 3561A dynamic signal analyzer* to obtain the spectra up to 100.000 kHz. By observing the height of the peaks and noise ground while changing something in the setup, the spectra gives information about the intensity noise. The less higher the peaks are or noise floor is, the less noisy is the signal.
However, a different approach was chosen. A digital oscilloscope, the *RS PRO IDS-2104E*, with digital output capability was used. One can easily connect a USB-stick with the oscilloscope and take the data of the current waveform as a CSV file for further data analysis.
The python library scipy and numpy was used in order to calculate the fast Fourier transform of the spectra. Taking care of the correct scales as well as the unit of the axis and choosing a logarithmic scale for the y axis one will find an equal looking spectra. To get an even better result, ten CSV files of the same spectra in AC mode were taken and averaged. Furthermore, to make it look even better, again 10 data points were summarised into one, so the curve is less sensitive to fluctuations. In fig. 5.1 is the resulting plot with the described method and a picture of the *HP 3561A* with the same incoming signal.

5.2 Experimental setup

The experimental setup for measuring intensity noise is simple, see fig. 6.1. In the original setup was a a lens after the laser diode followed by an anamorphic prism pair for beam shaping and another lens for focusing the beam on the photo diode. However, this can be neglected now. The measurement before the AOM is used as reference. The used fiber is a single mode fiber. So measuring after the fiber shouldn't produce a different result except for the lost of intensity. However, if the laser emits a mode which is not the single mode, it should be seen in the signal coming out of the fiber, so that was measured as well.
The used laser diode is a *EYP-DFB-1064-00080-1500-TOC03-0002* with 1064 nm wavelength [11].

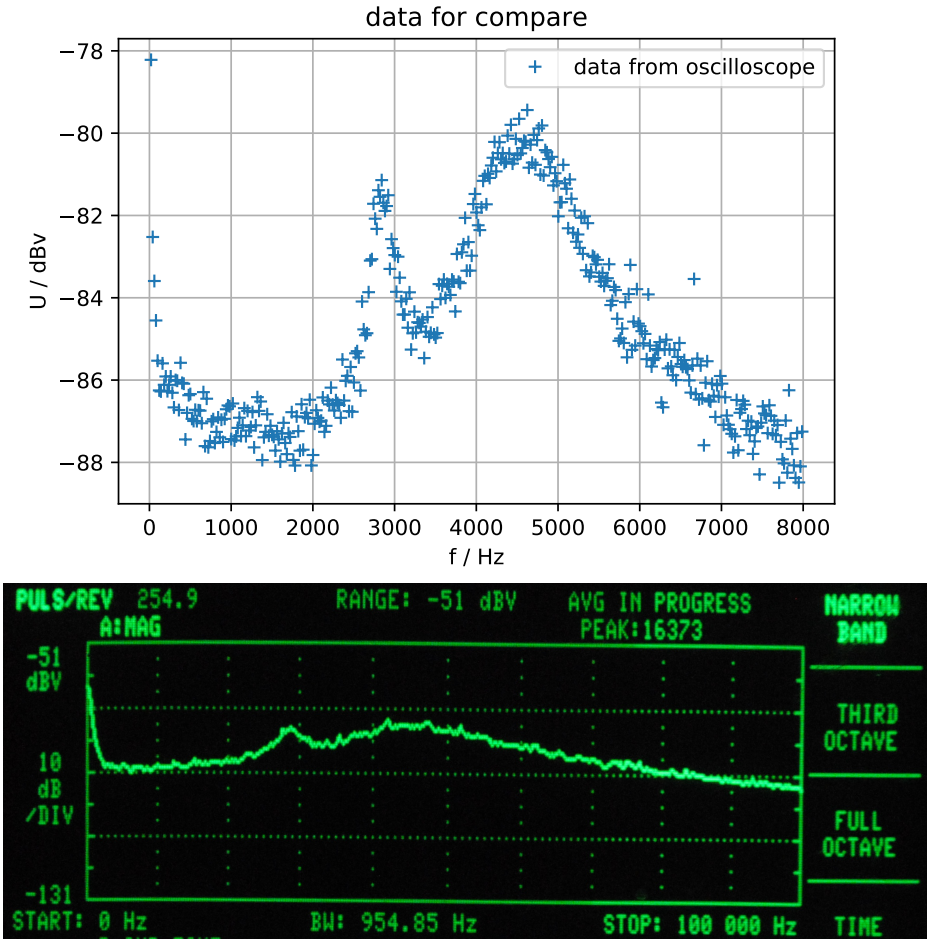

fig. 5.1: Comparison of the two methods

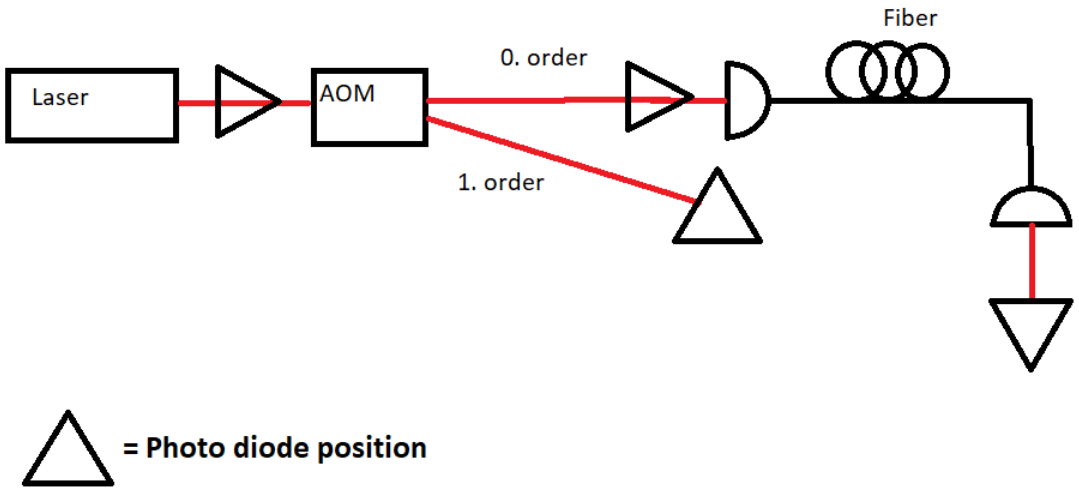

fig. 5.2: experimental setup for intensity noise measurement

5.3 Results

When adjusting the photo diode on every position showed in the experimental setup one gets the spectra shown in fig. 5.3. Here the output power of the laser was adjusted to 120 mA and a filter with ND = 3.0 is used. The RF source was provided by the the Marconi.
As expected the laser before the AOM shows the smallest amount of noise. The 0. and 1. order does not show much difference and the fiber adds again some noise. Note that the thickness of the fiber signal is also the biggest. Therefore, the possible problem of the laser diode emitting multiple modes can be excluded.

Now comparing the different RF devices. Before the AOM would not make any sense and after the fiber does not show any additional features, except for the general loss of power. So only the zeroth and first order are presented in fig. 5.4. Here again a current of 120 mA was used, but this time a filter with ND = 5.0. This explains the smaller y-values compared to fig. 5.3. There is no noticeable difference between the three devices. So they have not much effect on intensity noise.

5.4 Challenges and problems

Noise of the photo diode

The behavior of the photo diode in terms of the DC signal is not as expected. In fig. 5.5 one can see the different spectra for different DC valued. The labeling is as follows:

Label	Value
-1.0	0.5 V
-1.1	1 V
-1.2	2 V
-1.3	3 V
-1.4	4 V

From -1.0 to -1.1 it makes sense, because from 0.5 V to 1 V is 3 dB and one can see that difference on the right side of the plot. But the rest do not behave like expected. This might be an issue of the photo diode and its angle dependency.

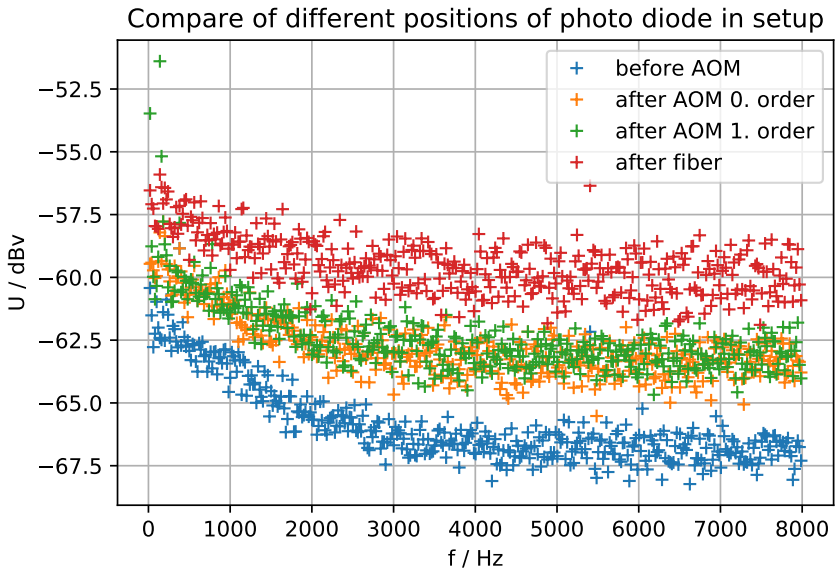

fig. 5.3: These are the raw spectra averaged over 10 CSV files, without dividing the dc value.

Saturation and angle of the photo diode

A *PDA05CF2* photo diode was used for the first measurement. This diode is very fast (150 MHz), but easy to get in saturation with this setup. First the diode laser was adjusted such that the DC value reached a point surely out of the danger of saturation. Actually the plots in fig. 5.1 are made in saturation. The first thought was that this peaks are noise of

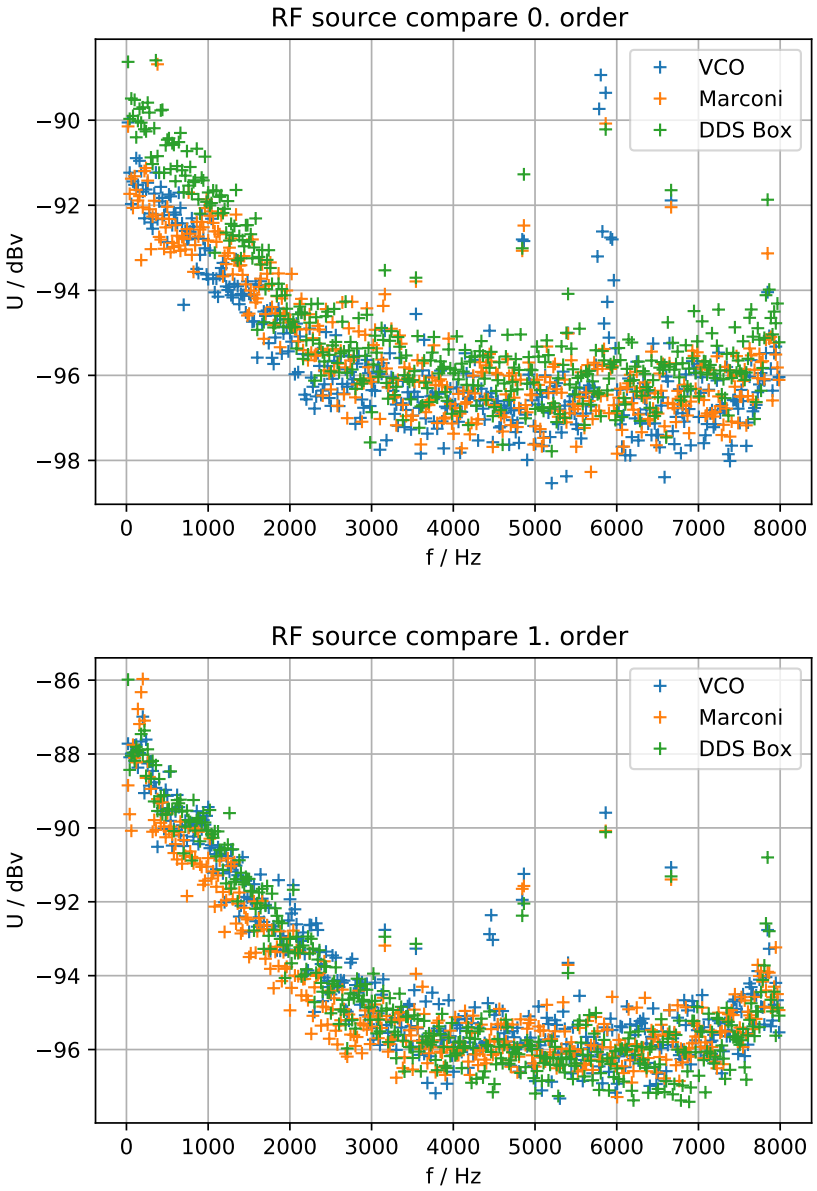

fig. 5.4: Comparing intensity noise of different RF sources with laser current I = 120 mA and a ND filter with ND = 5.0

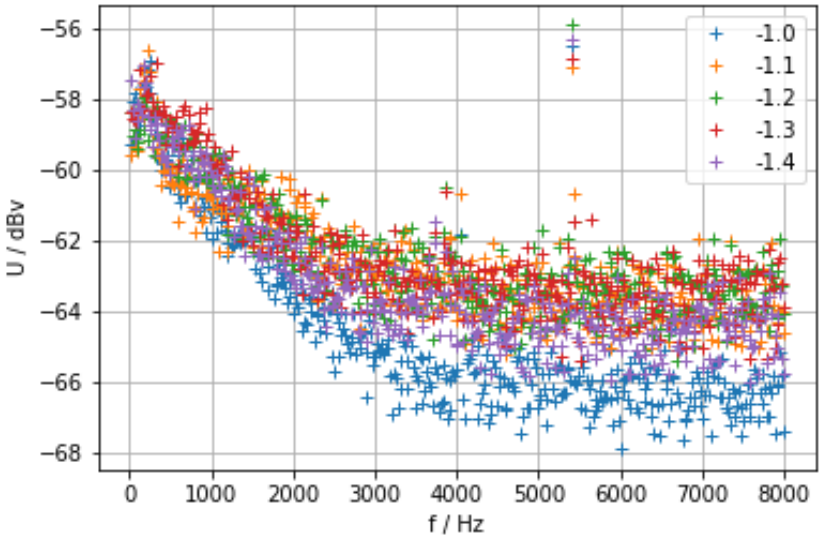

fig. 5.5: Different incoming DC on photo diode

the laser diode. However, if the photo diode was aligned correctly and the laser was barely emitting, there were no peaks. So it was clear, that the resonances are made by the photo diode and not by the laser. One possible reason for this resonances is that the enter of the photo diode has a reflective envelope causing resonances. This might also be the reason for the unexpected behavior seen in fig. 5.5.
After this discover optical attenuators were used as well as a different photo diode, namely the *DET36A/M*. This photo diode has a bigger active surface, but is not as fast as the last one, however still sufficient for this setup.

Fast Fourier transform (fft)

The spectra were calculated via a build in fft function in a scientific python library (scipy). These functions are great for have a quick idea about the Fourier transform. However, the correct scaling of the axis is not build in into the function. Dealing with the x axis is not a big problem since one just have to norm it manually, because of the symmetric complex spectra. The vertical axis causes more problems though. Actually is does not make much sense, but the value of the y axis seems to depend on the frequency its referring to. One possible reason for this problem is because the waves does not fulfil their full cycle. One way to fix this problem is the use of so called window functions. The SciPy library offers some of such functions. The idea behind window functions is to smooth the end of the measured spectra, such that the left and right end of the spectra has less impact on the Fourier transform.
However, since the spectra calculated without it looked the same as with the *HP 3561A* they were not used, so it is still possible to compare the spectra of the two methods. Furthermore,

because of the average over ten spectra and the fact that only the relevant change between the measurements is more important than the absolute values it is sufficient enough.

Overlapping signals

One has to be aware of the time it takes to get ten disjoint spectra with the oscilloscope. If two spectra overlap all frequencies in this cut set appear twice es often than the rest. This distorts the averaging, because it is not independent anymore.

6 Measuring phase noise

6.1 Measuring method and experimental setup

The chosen setup is basically the self-heterodyne method using only one laser presented in the phase noise section of the theoretical background (section 2.2.2). The only difference is the missing first beam splitter. Since the AOM by itself splits the beam, no additional beam splitter was used. This might have caused additional amplitude modulation on the signal.

The data sheet of the diode laser states a linewidth of 2 MHz [11]. Doing a generous estimate and assuming a linewidth of 1 MHz one can assume a coherence length of about 100 m (calculated with [22]). In order to be on the safe side 150 m were used. Here was another fast photo diode used again.

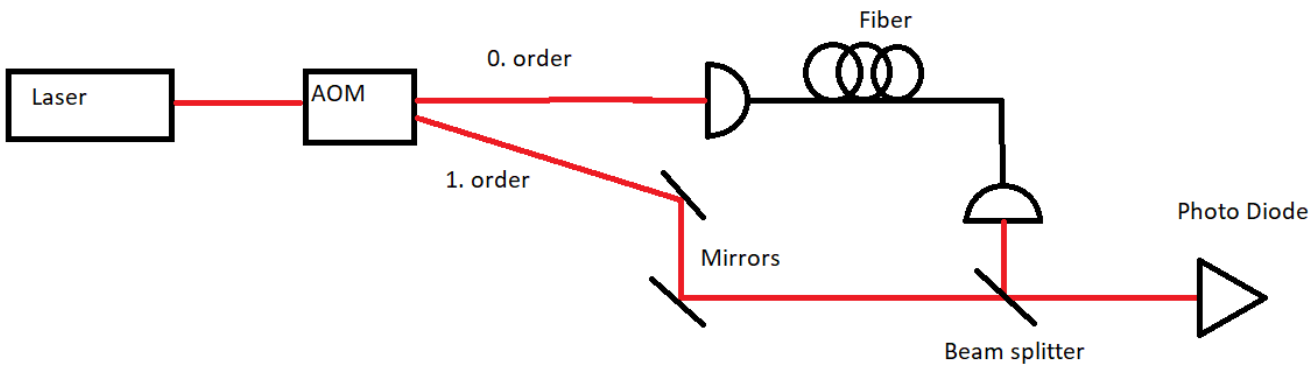

fig. 6.1: experimental setup for intensity noise measurement

6.2 Results

Measuring the beat note of all RF sources, with the large signal analyser again, one will find the spectra showed in fig. 6.2. Here the resolution and video bandwidth of the spectrum analyser was set to 100 Hz and it was averaged 10 times again. They all show more or less sharp peaks at the center and a brighter widening underneath it. All of these signals in on diagram is showed in top of fig. 6.3. Here once again one can see the slight frequency shift of the VCO like in fig. 4.4. The widening does not vary much with the different RF

sources. It always has a linewidth of around 20 kHz. for -80 dBm. However, the sharper peak shows more difference in the brightness. It shows the same tendency as the raw RF sources. The bottom diagram of fig. 6.3 shows the signal when the beam of the 1. order is blocked, so one only observes so called **amplitude modulation**, caused by the AOM the beam propagating through it. So this has nothing to do with interference. However, the amplitude modulation of the DDS Box peaks at about -70 dBm, while the beat note peaks at -20 dBm, even though the most intensity should be in the 0. order.

6.3 Challenges and problems

Amplitude modulation

Instead of a beam splitter the AOM was used. This should make no difference for the beat note, however, this might caused the unexpected height of the sharp peak. So using a beam splitter before the AOM could help to curb this effect.

Linewidth of the widening

The actual goal was to measure the linewidth of the laser itself. However the widening beneath the sharp peak had a linewidth of around 20 kHz. This is way smaller as expected, since the actual laser has a linewidth of 2 MHz.
One possible reason for this might be that the linewidth of the laser is in the order of 100 kHz so the 150 m of fiber are not enough to get out of the coherence. However, this is unlikely, since a diode laser with such a linewidth would be specified like this on the sheet and would be more expensive.

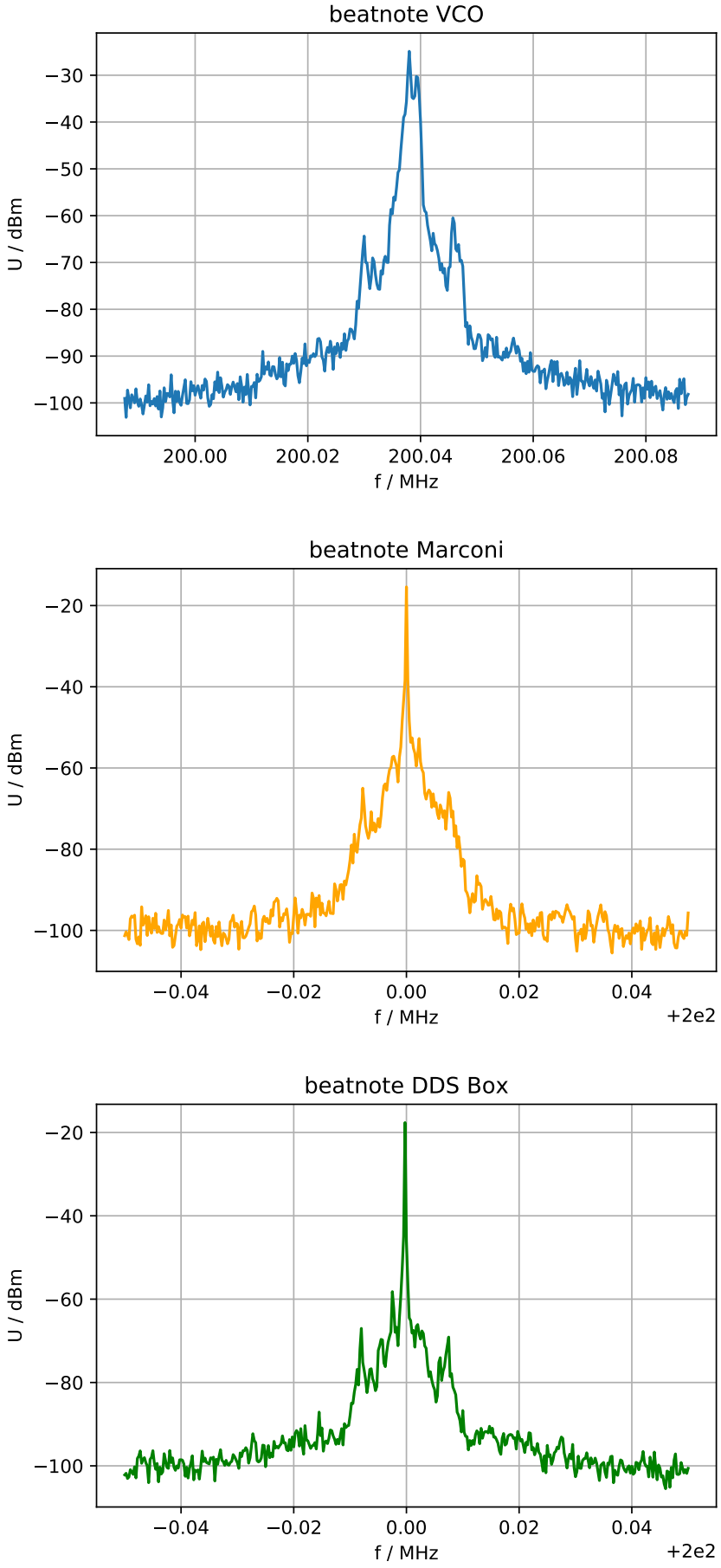

fig. 6.2: beat notes of all three signal generators

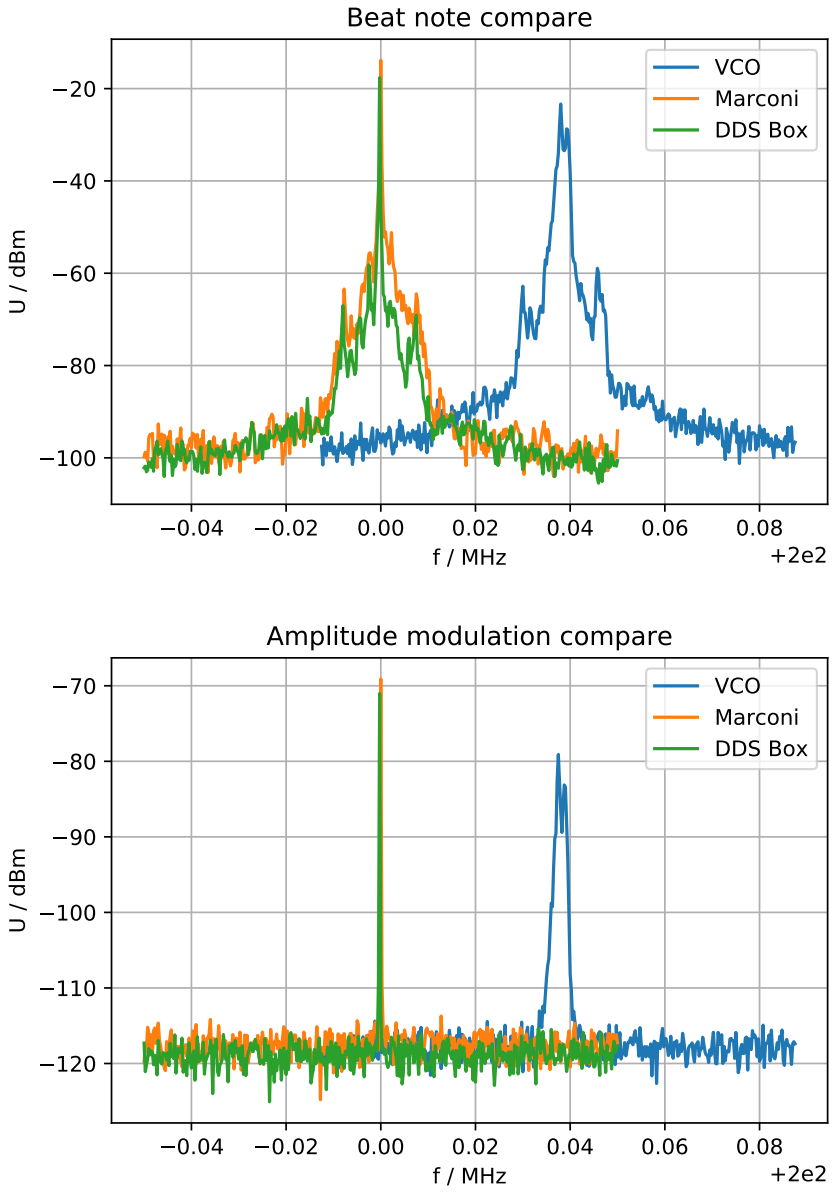

fig. 6.3: top: all three beat notes in one diagram
bottom: only the 0. order on the photo diode

7 Conclusion and Outlook

The first part of the thesis, which was building the DDS Box, was successfully finished. This Box can be used in future experiments having the need of stable RF signals.
The intensity noise of all three RF sources were compared with the conclusion that no improvement was achieved. However, it is no downgrade ether. So in term of intensity noise, the replacement of the old setup with the new DDS box combined with the amplifying circuits of Dr. Akos Hoffmann, achieved the same accuracy. It even saved space in the lab, since the DDS box is much smaller and has eight output channels and offers more features given by the AOM amplifying box. Additionally, this thesis showed which property of the VCO box caused the most problem in terms of stable RF signal.
The phase noise characterisation was not as successful as expected, since it was not possible to measure the actual linewidth of the laser. However, also here it was possible to show that the DDS box can compete with the current setup. So in terms of phase noise its again no downgrade.
Since the improvement of the intensity noise is not significant the new setup would not make lower temperatures possible. This problem needs to be addressed, because intensity noise causes exponential heating [25]. One way to address this issue is to introduce a PID circuit into the setup [5]. Since intensity fluctuations occur and disturb in the lower frequency spectrum it can be controlled by electronic circuits. The idea of a PID feedback loop is to compare an input signal, generated by a separated beam of the laser on a photo diode, with a wanted output signal. This circuit has to be a custom made one though, since it is needed for a large dynamic region. However, this would be the next step to achieve more stability, lower temperatures and thus a gate for new interesting physics.

8 Appendix

All plots used in this thesis are created with the open source python library matplotlib [15]. Also all the numerical calculations, optimization for fit, Fourier transform with SciPi [16].

8.1 Serial Peripheral Interface (SPI)

The serial peripheral interface (SPI) is a common used way to manage the communication between ICs. There are others like I^2C, UART, USB and much more. They all work differently and everyone has its own advantages and disadvantages.
SPI uses a master-slave protocol with (at least) 4 wires. The system clock (SCLK), master-out slave-in (MOSI), master-in slave-out (MISO), and slave select (SS). There is no real convention on the names though. The SS pin for example is also called chip enable (CE) or chip select (CS). The Raspberry Pi uses CE. The SCLK specifies the velocity in which every operation happens. The MOSI wire is for sending data from the master to the slave and MISO is for sending data from slave to master. The SS wire enables the communication between master and slaves. This is why SPI has at least 4 wires. This is illustrated in fig. . One can connect multiple slaves with the same SCLK, MOSI and MISO, but different

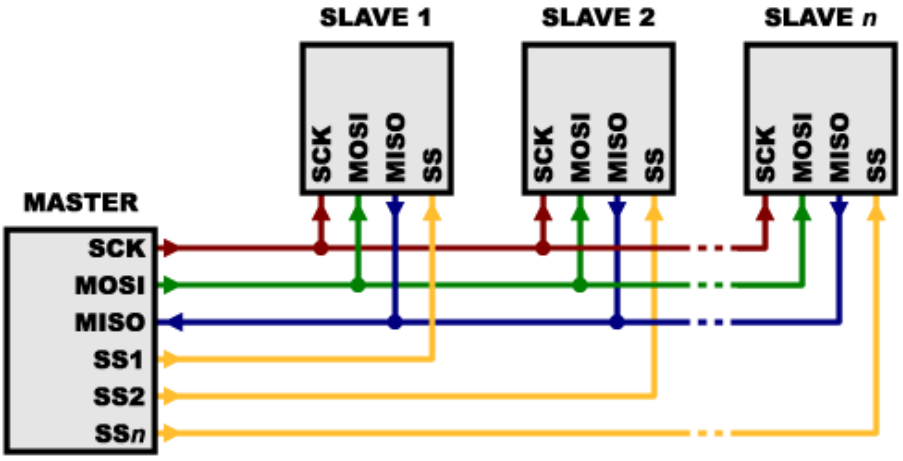

fig. 8.1: Basic structure of devices wired up with SPI [13].

SS. Therefore it was convenient to use SPI for this project. Every time the SCLK raises the voltage is set at the MOSI pin and measured at the MISO pin. But only if the SS is enabled. If the voltage is high thats a one and if it is low it is a zero. In this way one can transmit bits and therefore digital information.
Furthermore, it is fast and in this project it was clear which device will act as master, which has not to be specified with for example I^2C. Since there is no well-defined standard for the use of SPI one has to read the manual of the chip carefully. For example some chips have a max SCLK of 100 kHz and some of 100 MHz.
For more information about SPI or other ports see [14].

References

[1] Aeroflex. *Marconi signal generator 2024 data sheet*. https://www.matsolutions.com/Portals/0/Product%20documents/IFR%20(now%20Aeroflex)/2024/2024%20Operating%20Manual.pdf. [Online; accessed 22-September-2019].

[2] A. S. Arnold, J. S. Wilson, and M. G. Boshier. "A simple extended-cavity diode laser". In: *Review of Scientific Instruments* 69.3 (1998), pp. 1236–1239. DOI: 10.1063/1.1148756. eprint: https://doi.org/10.1063/1.1148756. URL: https://doi.org/10.1063/1.1148756.

[3] David Van Baak. "Noise Fundamentals NF1-A instructor's manual". In: 2010.

[4] MEAN WELL EUROPE B.V. *Data Sheet RS-15-5*. https://www.meanwell.com/webapp/product/search.aspx?prod=RS-15. [Online; accessed 21-September-2019].

[5] Prof. Jonathan Home Caspar Giehr Frieder Lindenfelser. "Laser Intensity Stabilisation". In: *Institute for Quantum Electronics, ETH Zurich* (May 27, 2014).

[6] Mini Circuits. *BBP-21.4+*. https://ww2.minicircuits.com/pdfs/BBP-21.4+.pdf. [Online; accessed 13-September-2019].

[7] Mini Circuits. *FD-2+*. https://ww2.minicircuits.com/pdfs/FD-2+.pdf. [Online; accessed 10-September-2019].

[8] Mini Circuits. *ZMSC-2-1+*. https://ww2.minicircuits.com/pdfs/ZMSC-2-1+.pdf. [Online; accessed 13-September-2019].

[9] Analog Devices. *Fundamentals of Direct Digital Synthesis (DDS)*. https://www.analog.com/media/en/training-seminars/tutorials/MT-085.pdf. [Online; accessed 18-August-2019]. 2009.

[10] E. A. Donley et al. "Double-pass acousto-optic modulator system". In: *Review of Scientific Instruments* 76.6 (2005), p. 063112. DOI: 10.1063/1.1930095. eprint: https://doi.org/10.1063/1.1930095. URL: https://doi.org/10.1063/1.1930095.

[11] eagleyard. *Laser Diode data sheet*. https://www.eagleyard.com/fileadmin/downloads/data_sheets/EYP-DFB-1064-00080-1500-TOC03-0002.pdf. [Online; accessed 23-September-2019].

[12] Thomas Erben. "Unix-Kommandos". In: *Einführung in Unix/Linux für Naturwissenschaftler: Effizientes wissenschaftliches Arbeiten mit der Unix-Kommandozeile*. Berlin, Heidelberg: Springer Berlin Heidelberg, 2017. ISBN: 978-3-662-50301-0. DOI: 10.1007/978-3-662-50301-0_4. URL: https://doi.org/10.1007/978-3-662-50301-0_4.

[13] Mike Grusin. *SPI Turorial*. https://learn.sparkfun.com/tutorials/serial-peripheral-interface-spi/all. [Online; accessed 19-August-2019].

[14] Paul Horowitz and Winfield Hill. *The art of electronics; 3rd ed.* Cambridge: Cambridge University Press, 2015. URL: https://cds.cern.ch/record/1981307.

[15] J. D. Hunter. "Matplotlib: A 2D graphics environment". In: *Computing in Science & Engineering* 9.3 (2007), pp. 90–95. DOI: 10.1109/MCSE.2007.55.

[16] Eric Jones, Travis Oliphant, Pearu Peterson, et al. *SciPy: Open source scientific tools for Python*. [Online; accessed 9/12/2019]. 2001-2019. URL: http://www.scipy.org/.

[17] K. G. Libbrecht and J. L. Hall. "A low-noise high-speed diode laser current controller". In: *Review of Scientific Instruments* 64.8 (1993), pp. 2133–2135. DOI: 10.1063/1.1143949. eprint: https://doi.org/10.1063/1.1143949. URL: https://doi.org/10.1063/1.1143949.

[18] Dr. Rüdiger Paschotta. *Data Sheet of the AD9959*. https://www.analog.com/media/en/technical-documentation/data-sheets/AD9959.pdf. [Online; accessed 18-September-2019].

[19] Dr. Rüdiger Paschotta. *Relativ Intensity Noise*. https://www.rp-photonics.com/relative_intensity_noise.html. [Online; accessed 15-September-2019].

[20] Dr. Rüdiger Paschotta. *Relaxation Oscillations*. https://www.rp-photonics.com/relaxation_oscillations.html. [Online; accessed 15-September-2019].

[21] Dennis V. Perepelitsa. "Johnson Noise and Shot Noise". In: 2006.

[22] RP Photonics. *Coherence Length calculator*. https://www.rp-photonics.com/coherence_length.html. [Online; accessed 23-September-2019].

[23] RP Photonics Consulting GmbH Rüdiger Paschotta. *Noise in Laser Technology – Part 1: Intensity and Phase Noise*. https://www.rp-photonics.com/article_noise_in_laser_technology1.html. [Online; accessed 12-September-2019].

[24] Bahaa E A Saleh and Malvin Carl Teich. *Fundamentals of photonics; 2nd ed.* Wiley series in pure and applied optics. New York, NY: Wiley, 2007. URL: https://cds.cern.ch/record/1084451.

[25] Tom Savard, K. O'Hara, and J. Thomas. "Laser-noise-induced heating in far-off resonance optical traps". In: *Physical Review A - PHYS REV A* 56 (Aug. 1997). DOI: 10.1103/PhysRevA.56.R1095.

[26] A. L. Schawlow and C. H. Townes. "Infrared and Optical Masers". In: *Phys. Rev.* 112 (6 1958), pp. 1940–1949. DOI: 10.1103/PhysRev.112.1940. URL: https://link.aps.org/doi/10.1103/PhysRev.112.1940.

[27] Keysight Technologies. *Data Sheet of ESA-E Series Spectrum Analyzer*. https://literature.cdn.keysight.com/litweb/pdf/5989-9815EN.pdf?id=1548393. [Online; accessed 15-September-2019].